On Interference Dynamics in Matérn Networks

Udo Schilcher, Jorge F. Schmidt, and Christian Bettstetter, *Senior Member, IEEE*

Abstract—A thorough understanding of the temporal dynamics of interference in wireless networks is crucial for the design of communication protocols, scheduling, and interference management. This article applies stochastic geometry to investigate the interference dynamics in a network of nodes that use carrier sense multiple access (CSMA). This type of network is approximated by a Matérn hard-core point process of type II with Nakagami fading. We derive and analyze expressions for the variance, covariance, and correlation of the interference power at an arbitrary location. Results show that even though the commonly used Poisson approximation to CSMA may have the same average interference as the Matérn model, the interference dynamics behaves significantly different. In this way, this study reveals a pitfall in the modeling of wireless systems and contributes to the theory of interference calculus.

Index Terms—Wireless networks, stochastic geometry, interference dynamics, correlation, Matérn point process, hard-core process, modeling pitfalls, Nakagami fading, CSMA

1 Introduction

1.1 Motivation

The modeling and analysis of interference in wireless networks by means of stochastic geometry [1] has become popular in the course of the past 15 years (see [2], [3], [4]). The majority of work in this domain uses simple modeling assumptions for reasons of mathematical tractability. A common network model includes uniformly randomly distributed nodes employing slotted ALOHA for medium access and Poisson arrival of transmission demands. This leads to uniformly distributed senders for interference analysis, which can be modeled by a Poisson point process (PPP). The PPP facilitates the derivation of mathematical expressions while retaining important network properties. Such networks are sometimes called *Poisson networks*; they are well understood in the communications theory community with several results available in the literature (see [3], [4], [5], [6], [7], [8], [9]).

In practice, however, many computer and communication networks do not access the shared medium in an ALOHA style but perform some type of *carrier sensing*. An example is Carrier Sense Multiple Access (CSMA), in which each node senses the medium and only starts to send a message if the medium is idle (otherwise backs off according to some rule and tries to send at a later instant) with the goal to reduce the number of message collisions. CSMA is also the basis for medium access control in IEEE 802.11 [10]. Although carrier sensing is not captured by Poisson networks, CSMA networks are approximated in most analytical studies by a Poisson network [11], [12], [13], [14], [15]. This approximation has been shown to be accurate for first-order statistics of the interference power, i.e., statistics at one point in space, such as expected value and variance (see [12], [13], [16]). Its suitability for higher-order statistics of interference (i.e., at several points in time or space) is, however, still unknown.

A better, very natural choice to model the senders in networks with carrier sensing is the Matérn hard-core point process (MPP) [17]. It introduces a guard circle around each sender in which no other node is allowed to send (see [3], [18]). This resembles the carrier sensing and is, in fact, suited for any kind of wireless network with spatial reservation of a transmission floor. It is still only an approximation for CSMA networks because real CSMA implementations are more complex. For example, there is a chance that two close nodes send simultaneously due to imperfect sensing or hidden terminal problems [19]. MPP assumes perfect sensing, thus leading to a slight underestimation of interference. Nevertheless, the approximation by MPP is much closer to CSMA than any PPP model and brings the theory of interference calculus a step forward in the direction of more realistic models. From a more general perspective, only few analytical results are available for MPPs, severely limiting the accurate analysis of many modern wireless technologies. The article at hand intends to fill this research gap with special emphasis on the stochastic analysis of interference dynamics.

1.2 Contributions

We derive expressions for the expected value, variance, covariance, and temporal correlation of the interference power at an arbitrary point in space in a network with carrier sensing modeled by an MPP of type II. Wireless links are modeled by a distance-dependent path loss and Nakagami small-scale fading. The derived expressions are analyzed to highlight the pitfalls of the popular Poisson approximation to CSMA and to explore the impact of system parameters on the correlation of interference. The main novelty is that

- *U. Schilcher is with the Institute of Networked and Embedded Systems, University of Klagenfurt, Lakeside B02a, 9020 Klagenfurt am Wörthersee, Austria, and also with Lakeside Labs GmbH, Lakeside B04b, 9020 Klagenfurt am Wörthersee, Austria. E-mail: udo.schilcher@aau.at.*
- *J.F. Schmidt is with Lakeside Labs GmbH, Lakeside B04b, 9020 Klagenfurt am Wörthersee, Austria. E-mail: schmidt@lakeside-labs.com.*
- *C. Bettstetter is with the Institute of Networked and Embedded Systems, University of Klagenfurt, Lakeside B02a, 9020 Klagenfurt am Wörthersee, Austria. E-mail: christian.bettstetter@aau.at.*

Manuscript received 7 June 2018; revised 22 Feb. 2019; accepted 9 Apr. 2019. Date of publication 15 Apr. 2019; date of current version 3 June 2020. (Corresponding author: Udo Schilcher.)
Digital Object Identifier no. 10.1109/TMC.2019.2911498

expressions for higher-order moments and correlation of interference have been unknown so far for Matérn networks. These measures show as to how interference changes over time: Is it changing strongly or weakly (variance)? Is it changing quickly or slowly (correlation)? Along these lines, our results give a deeper and more realistic understanding of the *temporal dynamics of interference* in wireless networks.

From a practical perspective, such understanding is useful in the design of communication protocols, scheduling, and interference management for many popular wireless technologies for which only rough approximations are available today. For example, a cooperative relaying protocol should take into account the correlation of interference to choose its relay. For instance, a higher correlation requires a higher number of potential relays [20]. As further example, LTE Release 13 specifies a licensed-assisted access (LAA) operation mode that includes a listen-before-talk channel sensing mechanism to support coexistence with Wi-Fi in the unlicensed spectrum (see [21], [22]). LAA is also perceived to be a key feature of 5G networks [23]. In order to properly design such a system, models like MPP are required.

Our scientific contributions are as follows:

- We derive expressions for the probabilities of one or two points in a PPP being retained in one or two independent Matérn thinnings of the PPP.
- We derive expressions for the expected value, variance, covariance, and temporal correlation of interference in Matérn networks.
- We show that interference correlation in Matérn networks is significantly different from that in Poisson networks, which leads to the qualitative conclusion that a PPP is unsuited to capture second-order properties of CSMA networks.
- We analyze the influence of the system parameters on the interference correlation and show that, in contrast to Poisson networks, it depends on the intensity of the MPP and the path loss exponent. Furthermore, fading has a stronger impact on the correlation in networks with carrier sensing.
- We state the potential use of the presented results in practical networks with carrier sensing.

1.3 Related Work

Related work mainly includes publications on the modeling of CSMA networks by means of stochastic point processes and publications on interference dynamics in wireless networks. Let us first revisit some work on the use of MPPs in the analysis of interference. The mean interference experienced by a node can be calculated by numerical integration [18]; an upper bound in terms of a closed-form expression is also available [24]. Considering network performance, a coverage analysis using a PPP approximation is done in [3], which is used to calculate the sensing sensitivity that maximizes the density of concurrent transmissions. Furthermore, the mean throughput [16] and capacity for high SIR [25] are calculated, and the impact of network parameters (e.g., minimum separation between nodes, path-loss exponent, and sensing threshold) on the mean throughput is investigated [26]. All these results have in common that they only consider first-order statistics to analyze the network, i.e., they analyze interference at a single point in time and space. Hence, these results are incapable of capturing the dynamics of interference. In contrast, we quantify the dynamics of interference (in terms of temporal correlation), which is essential to evaluate a wide range of communication methods, e.g., diversity techniques [6] and multiple input multiple output (MIMO) in millimeter wave communications [27].

Networks with carrier sensing are also modeled with soft-core point processes [28], [29], [30]. Unlike hard-core point processes, there is no strict minimum distance between senders. Instead, a repelling force between senders is assumed that is stronger if they are closer to each other. Hence, it is unlikely for two senders to be very close to each other, yet it is not impossible. This resembles a form of imperfect carrier sensing [28]. Although soft-core processes are probably even more realistic models for CSMA networks, they are rarely applied due to the lack of analytical results.

Alternative models for CSMA networks include perturbed triangular lattices [31] and sequential spatial inhibition (SSI) processes [32]. These alternatives are investigated almost exclusively by simulations with almost no analytical results available.

The temporal and spatial correlation of interference restricted to PPPs is studied in [8], [9], [20], [33], and [34].

The article is structured as follows: Section 2 explains the system model, including node placement, wireless channel, and interference. Section 3 derives expressions for the mean value, variance, covariance, and correlation of interference. Section 4 analyzes the interference correlation and compares results to a Poisson network. Section 5 concludes the article.

2 Network Model

2.1 Spatial Distribution of Senders

The potential senders in a wireless network are distributed according to a PPP $\Phi_{\mathrm{p}} \subset \mathbb{R}^2$ with intensity λ_{p}. Time is partitioned into slots of equal duration. In each slot t, some of the potential senders act as senders, i.e., they transmit some data. These senders are modeled by an MPP of type II, denoted by $\Phi \subseteq \Phi_{\mathrm{p}}$.

Note that we do not consider the receivers; they are neither included in Φ nor in Φ_{p}. Instead, we assume that each sender has an associated receiver within its range similar to the Poisson bipolar network model ([35], [36]).

The decision of a potential sender about sending in a slot t is based on a sensing mechanism for medium access. This mechanism should prevent two nodes from simultaneously sending if their distance is below a certain threshold d, which is similar to CSMA [3]. This behavior is modeled, in each slot, by a dependent thinning of Φ_{p}, resulting in an MPP of type II with intensity λ for the senders. In other words, the selection of senders is done independently per slot by performing a Matérn thinning of a PPP in each slot.

Such Matérn type II thinning works as follows [1]: Each node $x \in \Phi_{\mathrm{p}}$ draws a uniformly i.i.d. random mark $m_x \sim \mathbb{U}(0,1)$. Node x is retained if and only if m_x is smaller than the marks m_y of all points $y \in \mathcal{C}(x,d)$, where $\mathcal{C}(x,r) = \{y \in \mathbb{R} \,|\, \|x-y\| \leq r\}$ is a circle with radius r centered at x.

Matérn point processes of type II are well suited to model networks with carrier sensing for the following reasons: As opposed to Poisson cluster processes (e.g., Matérn or Thomas

cluster processes), a Matérn hard-core process is introducing a minimum distance between each pair of concurrently sending nodes. By doing so, it avoids co-located nodes to send simultaneously similar to carrier sensing. Furthermore, due to its construction, Matérn hard-core processes of type II are especially well suited to model medium access control, since the random nature of Matérn thinning is realistically modeling the random selection of the nodes that are allowed to send. For example, when two co-located nodes try to send, the node sending first is selected due to random backoff leading to a different result every time this situation occurs. The same holds for the Matérn thinning.

The mechanism is fair in the sense that all potential senders are treated equally due to the stationarity of the MPP. It needs to be mentioned that, in real CSMA networks, there is still a possibility that nodes arbitrarily close to each other start sending simultaneously due to imperfect sensing, e.g., due to the hidden terminal problem [19]. This effect is not covered by the Matérn model and is outside the scope of this work.

2.2 Wireless Channel

The radio propagation is modeled by distance-dependent path loss and small-scale fading caused by multipath propagation. All nodes transmit with unit power. The power p received at the origin o from a sender x is given by $p = h_x^2\, \ell(\|x\|)$. The term $\ell(\|x\|) = \min(1, \|x\|^{-\alpha})$ is the distance-dependent path gain with exponent $\alpha > 2$. This specific path loss is adopted to avoid a singularity for the distance approaching zero as occurs in the commonly used singular path loss model. This non-singularity is important as otherwise the second moment of interference was infinite (and all higher moments as well) [8], and thus could not be used to calculate the correlation of interference. The random variable h_x^2 models small-scale fading, and we assume fading to be independent for different nodes and for different time slots. We employ the versatile Nakagami-m fading model [37], for which the random variable h_x^2 follows a gamma distribution with parameter m, i.e., $h_x^2 \sim \Gamma(m, \frac{1}{m})$ with mean $\mathbb{E}[h_x^2] = 1$. Recall that the Nakagami model also covers Rayleigh fading ($m = 1$) and no fading ($m \to \infty$).

2.3 Interference

We are interested in the overall interference at an arbitrary location. Due to the stationarity of the point processes involved we consider, without loss of generality, the interference at the origin o. This model can be used for a scenario in which the node suffering from the interference is not an inherent part of the network that causes it. An example application is mmWave base stations within a 5G cellular network [38] that are interfered by the cellular system without being part of it.

The interference power at time t_i (time index i) is calculated as the sum of the signal powers arriving at the origin o from all active senders, i.e.,

$$I_i = \sum_{x \in \Phi_\mathrm{p}} h_x^2\, \ell(\|x\|) \gamma_x(t_i) = \sum_{x \in \Phi(t_i)} h_x^2\, \ell(\|x\|), \tag{1}$$

where $\gamma_x(t_i)$ indicates whether a node x is retained by Matérn thinning at time t_i, i.e., whether it sends at t_i.

3 Interference Expressions

Our overall goal is to derive the temporal correlation of interference in a given point in space in a Matérn network in terms of Pearson's correlation coefficient $\rho[I_1, I_2]$. As a basic ingredient for the correlation, the probabilities of a point being retained by the Matérn thinning is required.

3.1 Retainment Probabilities

The retainment probabilities derived in the following are the probabilities that a node survives the Matérn thinning once or twice, or that two nodes survive it in the same or different thinnings. In a wireless network they model the probability that a node which has a message to send is actually able to transmit it at a given time. This is related to the carrier sensing, i.e., whether the channel is sensed idle or busy.

Let p_1 and p_{12} denote the probability that a point is retained once or twice, respectively, and $p_{1/1}(r)$ and $p_{1/2}(r)$ denote the probability that two different points at distance r are retained in one or two thinnings, respectively.

Lemma 1 (Single point is retained once). *The probability that a point $x \in \Phi_\mathrm{p}$ is retained by Matérn thinning is [1]*

$$p_1 = \frac{1 - \exp(-\lambda_\mathrm{p}\, d^2\pi)}{\lambda_\mathrm{p}\, d^2\pi}, \tag{2}$$

where $d^2\pi$ is the area of a circle with radius d representing the sensing area of a node.

A proof of this lemma is given in [1] and [39].

Remarks.

- It immediately follows that [1]

$$\lambda = \lambda_\mathrm{p}\, p_1 = \frac{1 - \exp(-\lambda_\mathrm{p}\, d^2\pi)}{d^2\pi}. \tag{3}$$

- The theoretical maximum intensity of an MPP for a given d is $\lim_{\lambda_\mathrm{p} \to \infty} \lambda = \frac{1}{d^2\pi}$. Every node possesses an empty guard area of $d^2\pi$. This point process is sometimes criticized for having low intensities [32], but it can actually achieve λ up to this limit if one chooses a large enough PPP intensity λ_p.
- For $d \to \infty$ the probability that a point is retained vanishes, i.e., $\lim_{d \to \infty} p_1 = 0$. For $d \to 0$ all points are retained, i.e., $\lim_{d \to 0} p_1 = 1$.

Lemma 2 (Single point is retained twice). *The probability that a point $x \in \Phi_\mathrm{p}$ is retained twice by two independent Matérn thinnings is*

$$p_{12} = \frac{\exp(-\lambda\, d^2\pi)\big(E_i(\lambda\, d^2\pi) - \log(\lambda\, d^2\pi) - \gamma_\mathrm{Euler}\big)}{\lambda\, d^2\pi}, \tag{4}$$

where $E_i(x)$ denotes the exponential integral function and $\gamma_\mathrm{Euler} \approx 0.577216$ is Euler's γ constant.

A proof of this lemma is given in Appendix A.

Remarks.

- The probability p_{12} that a given point x is retained twice is not the retaining probability squared, i.e.,

$p_{12} \neq p_1^2$ for all $d > 0$. The reason is that the number of neighboring points that are potential "killers" of x is different for any $x \in \Phi_\mathrm{p}$ but stays constant over time. Hence, the retainment of x in different thinnings is correlated.

- We have $p_{12} > p_1^2$ for all $d > 0$, i.e., a point retained once is more likely to be retained a second time. This fact can be explained by the following intuition: A point x that is retained once has, on average, fewer neighboring points that could have potentially killed x. Therefore, in another independent thinning it has higher chances of being retained. In the limit, the probabilities converge to $\lim_{d\to\infty} p_1 = \lim_{d\to\infty} p_{12} = 0$.
- The intensity of points retained twice is $\lambda_\mathrm{p}\, p_{12}$.
- For $d \to 0$ all points are retained twice in two independent thinnings, i.e., $\lim_{d\to 0} p_{12} = 1$.

Lemma 3 (Two distinct points are retained in one thinning). *The probability that two points separated by a distance r are both retained in a Matérn thinning is (see [1], [39])*

$$p_{1/1}(r) = \frac{2\Gamma_d(r)\big(1-\exp(-\lambda\, d^2\pi)\big)}{\lambda^2 d^2\pi\Gamma_d(r)\big(\Gamma_d(r)-d^2\pi\big)} - \frac{2\big(1-\exp(-\lambda\Gamma_d(r))\big)}{\lambda^2\Gamma_d(r)\big(\Gamma_d(r)-d^2\pi\big)}, \tag{5}$$

for $r > d$ and 0 otherwise. Here, $\Gamma_d(r)$ is the area covered by two overlapping circles with radius d and centers separated by r, which is given by

$$\Gamma_d(r) = 2d^2\pi - \gamma_d(r). \tag{6}$$

The overlapping area of these two circles is

$$\gamma_d(r) = 2d^2 \arccos\Big(\frac{r}{2d}\Big) - \frac{r}{2}\sqrt{4d^2-r^2}, \tag{7}$$

for $r \leq 2d$ and 0 otherwise [1].

A proof of this lemma is given in Appendix A.

Remarks.

- From (5), we can calculate the second-order product density of the MPP by $\rho^{(2)}(r) = \lambda_\mathrm{p}^2\, p_{1/1}(r)$. A plot of it is shown in Fig. 1.
- For the case $r > 2d$ we have $\gamma_d(r) = 0$ and hence $\rho^{(2)}(r) = \lambda^2$, since $p_{1/1}(r) \overset{r\geq 2d}{=} p_1^2$. This implies that two points that are further than $2d$ from each other are independently retained or removed. Recall that the second-order product density for PPPs is λ_p^2.
- For the case $d < r \leq 2d$ the integration over $\rho^{(2)}(r)$ yields no closed form solution due to the complexity of $\gamma_d(r)$. Hence, in some cases it might be advantageous to approximate it by $\gamma_d(r) \approx d^2\pi - 2dr$ [1].

Lemma 4 (Two distinct points are retained in independent thinnings). *The probability $p_{1/2}(r)$ that a point $x \in \Phi_\mathrm{p}$ is retained by a thinning and $y \in \Phi_\mathrm{p}$ is retained in another, independent thinning with $r = \|x-y\| > 0$ is given in (8) for $r \geq d$ and in (9) for $r < d$.*

A proof of this lemma is given in Appendix A.

Remarks.

- The probability $p_{1/1}(r)$ vanishes for $r < d$ since two points closer than d cannot both be retained in one thinning. However, the probability that each of them is retained in an independent thinning is $p_{1/2}(r) > 0$ for $r < d$. Still, it is much smaller than for $r \geq d$ (see Fig. 1) since for $r \geq d$ they are neighbors and could potentially kill each other, i.e., the random number of neighbors is higher by one in this case.
- If the two points approach each other and become identical, $p_{1/2}(r)$ becomes the probability p_{12} that one point is retained twice, i.e., $\lim_{r\to 0} p_{1/2}(r) = p_{12}$. Care has to be taken when calculating this limit: We have to adopt (8), which is intended for $r \geq d$ and does not consider an extra point in the neighborhood. Hence, in the limit when the two points merge, there is no extra point in the neighborhood leading to (4). Calculating the limit of (9) leads to the different expression $\frac{\exp(-\lambda\, d^2\pi)(1+E_i(\lambda\, d^2\pi)-\log(\lambda\, d^2\pi)-\gamma_\mathrm{Euler})-1}{\lambda\, d^2\pi}$.
- If $r > 2d$, the events that two points are retained each in an independent thinning are independent. Therefore, we have $p_{1/2}(r) \overset{r\geq 2d}{=} p_1^2$.

Note that for $d \to 0$ all results in this section converge to the corresponding results of a PPP.

$$p_{1/2}(r) \overset{r\geq d}{=} \frac{\exp\Big(-\frac{d^4\pi^2\lambda_\mathrm{p}}{\gamma_d(r)}\Big)\left(2\Gamma\Big(0, d^2\pi\lambda_\mathrm{p}\Big(1-\frac{d^2\pi}{\gamma_d(r)}\Big)\Big) - \Gamma\Big(0, -\frac{d^4\pi^2\lambda_\mathrm{p}}{\gamma_d(r)}\Big) - \Gamma\left(0, -\frac{\lambda_\mathrm{p}\big(\gamma_d(r)-d^2\pi\big)^2}{\gamma_d(r)}\right)\right)}{\lambda_\mathrm{p}\,\gamma_d(r)} \tag{8}$$

$$\begin{aligned} p_{1/2}(r) \overset{r\leq d}{=}\ & \frac{\exp\Big(-d^2\pi\lambda_\mathrm{p}\Big(2+\frac{d^2\pi}{\gamma_d(r)}\Big)\Big)}{d^2\pi\lambda_\mathrm{p}^2\gamma_d^3(r)}\Bigg(\exp(2d^2\pi\lambda_\mathrm{p})\Big(\gamma_d(r)\big(1+2d^2\pi\lambda_\mathrm{p}-\gamma_d(r)\lambda_\mathrm{p}\big)-d^4\pi^2\lambda_\mathrm{p}\Big) \\ & \left(2E_i\left(d^2\pi\lambda_\mathrm{p}\left(\frac{d^2\pi}{\gamma_d(r)}-1\right)\right) - E_i\left(\frac{d^4\pi^2\lambda_\mathrm{p}}{\gamma_d(r)}\right) - E_i\left(\frac{\lambda_\mathrm{p}\big(\gamma_d(r)-d^2\pi\big)^2}{\gamma_d(r)}\right)\right) \\ & - \gamma_d(r)\exp\left(\frac{d^4\pi^2\lambda_\mathrm{p}}{\gamma_d(r)}\right)\Big(\exp(\lambda_\mathrm{p}\gamma_d(r))d^2\pi + \exp(2d^2\pi\lambda_\mathrm{p})(d^2\pi-2\gamma_d(r)) - 2\exp(d^2\pi\lambda_\mathrm{p})\big(d^2\pi-\gamma_d(r)\big)\Big)\Bigg). \end{aligned} \tag{9}$$

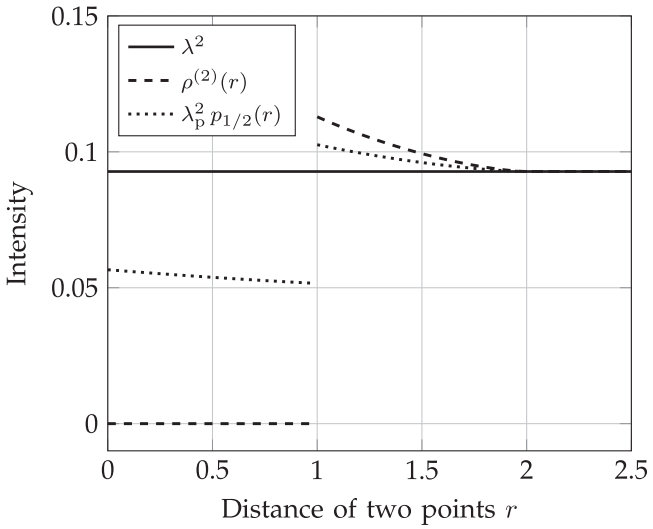

Fig. 1. Intensity of the MPP λ^2 (not a function of r), of two points separated by r retained in the same thinning $\rho^{(2)}(r)$ (the second-order product density), and of two points separated by r each retained in an independent thinning $\lambda_p^2\, p_{1/2}(r)$. Parameters are $\lambda_p = 1$ and $d = 1$.

3.2 Expected Value, Variance, and Covariance of Interference

The expected value of interference is a basic property and provides an underlying fairness metric. In all our comparisons we ascertain that all models lead to the same expected interference. Expressions for variance and covariance have a value on their own, and serve as intermediate results in the calculation of the correlation coefficient.

Lemma 5 (Expected interference). *The expected value of interference is*

$$\mathbb{E}[I] = \lambda\, \frac{\alpha\pi}{\alpha - 2}. \tag{10}$$

A proof of this lemma is shown in Appendix A.

Remarks.

- The expected interference (10) for MPP is the same as the one for PPP (given in [4], [33]) with the same process intensity using the same path loss model.
- The expression (10) does not correspond to the expected interference derived by Haenggi for MPP [18]. The core difference is in the modeling assumptions: Haenggi assumes that a node is located at the origin; his result thus represents the expected interference experienced by a typical node in the network. This assumption causes some mathematical difficulties, as the reduced Palm distribution has to be adopted. We do not assume a node to be located at the origin; all results hold for any point in space. Nevertheless, a data sink could be located at this point that neither sends data nor participates in the CSMA protocol. Along these lines, our assumptions are well-suited for a multipoint-to-point data collection scenario.

Theorem 1 (Variance of interference). *The variance of interference at the origin o is*

$$\begin{aligned}\mathrm{var}[I] = \lambda\, \frac{(m+1)\,\alpha\pi}{m\,(\alpha-1)} + 8\pi \int_{\frac{d}{2}}^{\infty} \int_0^{\infty} \int_0^{2\pi} \ell(r(\cosh\mu + \cos\nu))\\ \ell(r(\cosh\mu - \cos\nu))\, \frac{r^2}{2}\, (\cosh 2\mu - \cos 2\nu)\, \mathrm{d}\nu\, \mathrm{d}\mu\\ \rho^{(2)}(2r)\, r\, \mathrm{d}r - \left(\frac{\lambda\alpha\pi}{\alpha-2}\right)^2,\end{aligned} \tag{11}$$

where λ is the intensity of the MPP, m is the parameter of Nakagami fading, α is the path loss exponent, d is the hard-core distance, and $\ell(\cdot)$ is the path gain function.

Proof. We start by calculating the second moment of interference at time t by

$$\begin{aligned}\mathbb{E}\big[I^2\big] &= \mathbb{E}\left[\left(\sum_{x\in\Phi_p} h_x^2\, \ell(\|x\|)\gamma_x(t)\right) \cdot \left(\sum_{y\in\Phi_p} h_y^2\, \ell(\|y\|)\gamma_y(t)\right)\right]\\ &\overset{(a)}{=} \mathbb{E}\left[\sum_{x\in\Phi_p} \big(h_x^2\, \ell(\|x\|)\big)^2 \gamma_x(t)\right]\\ &\quad + \mathbb{E}\left[\sum_{x,y\in\Phi_p}^{\neq} h_x^2\, \ell(\|x\|) h_y^2\, \ell(\|y\|)\gamma_x(t)\gamma_y(t)\right],\end{aligned} \tag{12}$$

where in (a) terms with $x = y$ are separated from terms with $x \neq y$. The first of these expected values yields

$$\begin{aligned}\mathbb{E}\left[\sum_{x\in\Phi_p} \big(h_x^2\, \ell(\|x\|)\big)^2 \gamma_x(t)\right] &\overset{(a)}{=} \lambda_p p_1\, \mathbb{E}\big[h_x^4\big] \int_{\mathbb{R}^2} \ell^2(\|x\|)\, \mathrm{d}x\\ &= \lambda\, \frac{(m+1)\,\alpha\pi}{m\,(\alpha-1)},\end{aligned} \tag{13}$$

where we apply Campbell's theorem in (a) . The last expectation of (12) gives

$$\begin{aligned}&\mathbb{E}\left[\sum_{x,y\in\Phi_p}^{\neq} h_x^2\, \ell(\|x\|) h_y^2\, \ell(\|y\|)\gamma_x(t)\gamma_y(t)\right]\\ &\overset{(a)}{=} \int_{\mathbb{R}^2}\int_{\mathbb{R}^2} \ell(\|x\|)\, \ell(\|y\|)\, \rho^{(2)}(\|x-y\|)\, \mathrm{d}x\, \mathrm{d}y\\ &\overset{(b)}{=} 4\int_{\mathbb{R}^2}\int_{\mathbb{R}^2} \ell(\|x\|)\, \ell(\|x-2a\|)\, \rho^{(2)}(\|2a\|)\, \mathrm{d}x\, \mathrm{d}a\\ &\overset{(c)}{=} 4\int_{\mathbb{R}^2}\int_{\mathbb{R}^2} \ell(\|x+a\|)\, \ell(\|x-a\|)\, \mathrm{d}x\, \rho^{(2)}(\|2a\|)\, \mathrm{d}a\\ &\overset{(d)}{=} 8\pi \int_{\frac{d}{2}}^{\infty}\int_{\mathbb{R}^2} \ell\left(\left\|x + \begin{pmatrix} r\\ 0\end{pmatrix}\right\|\right) \ell\left(\left\|x - \begin{pmatrix} r\\ 0\end{pmatrix}\right\|\right) \mathrm{d}x\, \rho^{(2)}(2r)\, r\, \mathrm{d}r.\end{aligned} \tag{14}$$

In (a) we apply a basic property of the second-order product density $\rho^{(2)}(r) = \lambda_p^2\, p_{1/1}(r)$ [1, p. 112], where $p_{1/1}(r)$ is the probability that two points at distance r are both retained, as derived in Lemma 3. Furthermore, the expected values of the fading coefficients $\mathbb{E}\big[h_z^2\big] = 1$ for any $z \in \Phi_p$ are substituted. In (b) we substitute $y = x - 2a$, and 4 is the corresponding Jacobi determinant. In (c) we substitute $x + a$ for x. In (d) we substitute polar coordinates. The integration of r starts at $\frac{d}{2}$ as $\rho^{(2)}(r) = 0$ for $r < d$. Furthermore, we apply a rotation of the coordinate system to translate a into a real number a':

$$\mathbf{x}' = \begin{pmatrix} \cos\phi & \sin\phi \\ -\sin\phi & \cos\phi \end{pmatrix}\mathbf{x}, \tag{15}$$

where $\mathbf{x}'$ and $\mathbf{x}$ are the vector notations of points x' and x in $\mathbb{R}^2$, respectively, and $\phi = \arctan(a_I/a_R)$ is the phase of the polar coordinate of a. This transformation does not change the norms $\ell(\|x+a\|)$, $\ell(\|x-a\|)$, and $\ell(\|2a\|)$ involved in the integration, which can be verified by writing $x' = e^{j\phi}x$ and $a' = e^{j\phi}a$.

For an arbitrary but fixed $r \in \mathbb{R}$, the inner integral of (14) is

$$\int_{\mathbb{R}^2} \ell(\|x+a\|)\,\ell(\|x-a\|)\,\mathrm{d}x \overset{(a)}{=} \int_0^{\infty}\int_0^{2\pi} \ell(r(\cosh\mu + \cos\nu)\,\ell(r(\cosh\mu - \cos\nu)\frac{r^2}{2}\big(\cosh 2\mu - \cos 2\nu\big)\,\mathrm{d}\nu\,\mathrm{d}\mu. \tag{16}$$

In (a) we substitute elliptic coordinates defined as

$$\begin{aligned} x_1 &= r\,\cosh\mu\,\cos\nu \\ x_2 &= r\,\sinh\mu\,\sin\nu, \end{aligned} \tag{17}$$

and its corresponding Jacobi determinant $\frac{r^2}{2}\big(\cosh 2\mu - \cos 2\nu\big)$, and calculate the corresponding norms. Calculating $\mathrm{var}[I] = \mathbb{E}[I^2] - \mathbb{E}[I]^2$ yields the result. □

Remarks.

- The variance of interference is presented in terms of integral expressions that are solved numerically as there is no closed-form solution. The problematic term for symbolic integration is the second-order product density $\rho^{(2)}(r)$.
- Since numerical integration is involved in calculating the variance of interference some steps of the proof would not be needed. For example, the expression in step (a) of (14) could directly be solved numerically. However, it turns out that it is advantageous to rather solve the integration in (11) as it results in better numerical stability.
- The substitution of elliptic coordinates might also be interesting for other applications: It allows to solve integrations of the form $\int_{\mathbb{R}^2} \|x-a\|\|x+a\|\,\mathrm{d}x$, which sometimes occur in the derivation of second-order statistics of interference for both PPP and MPP.
- For $d \to 0$ the variance converges to the Poisson case: In (14) (a) the second-order product density $\rho^{(2)}(r)$ could be substituted by λ^2 leading to

$$\begin{aligned} &\mathbb{E}\left[\sum_{x,y\in\Phi_\mathrm{p}}^{\neq} h_x^2\,\ell(\|x\|)h_y^2\,\ell(\|y\|)\gamma_x(t)\gamma_y(t)\right] \\ &\quad= \left(\lambda\int_{\mathbb{R}^2}\ell(\|x\|)\,\mathrm{d}x\right)^2 \\ &\quad= \left(\lambda\,\frac{\alpha\pi}{\alpha-2}\right)^2. \end{aligned} \tag{18}$$

Since this expression is equal to $\mathbb{E}[I]^2$, we have

$$\mathrm{var}[I] = \lambda\,\frac{(m+1)\,\alpha\pi}{m\,(\alpha-1)}, \tag{19}$$

equal to the Poisson case [8].

Theorem 2 (Covariance of interference). *The temporal covariance of interference at the origin o is*

$$\begin{aligned} \mathrm{cov}\,[I_1, I_2] &= \lambda_\mathrm{p} p_{12}\,\frac{\alpha\pi}{\alpha-1} \\ &+ 8\pi\int_0^{\infty}\int_0^{\infty}\int_0^{2\pi} \ell(r(\cosh\mu + \cos\nu)) \\ &\ell(r(\cosh\mu - \cos\nu))\,\frac{r^2}{2}\big(\cosh 2\mu - \cos 2\nu\big)\,\mathrm{d}\nu\,\mathrm{d}\mu \\ &p_{1/2}(2r)\,r\,\mathrm{d}r - \left(\frac{\lambda\alpha\pi}{\alpha-2}\right)^2, \end{aligned} \tag{20}$$

where λ_p is the intensity of the PPP, $\lambda = \lambda_\mathrm{p} p_1$ is the intensity of the MPP, m is the parameter of Nakagami fading, α is the path loss exponent, d is the hard-core distance, and $\ell(\cdot)$ is the path gain function. $p_{1/2}(r)$ denotes the probability that two different nodes are retained in two independent Matérn thinnings, given in Lemma 4.

Proof. The proof goes along the lines of the proof of Theorem 1. We start by calculating the covariance of interference at times t_1 and t_2 by

$$\begin{aligned} \mathbb{E}[I_1 I_2] &= \mathbb{E}\left[\left(\sum_{x\in\Phi_\mathrm{p}} h_x^2\,\ell(\|x\|)\gamma_x(t_1)\right)\cdot\left(\sum_{y\in\Phi_\mathrm{p}} h_y^2\,\ell(\|y\|)\gamma_y(t_2)\right)\right] \\ &\overset{(a)}{=} \mathbb{E}\left[\sum_{x\in\Phi_\mathrm{p}} \ell^2(\|x\|)\gamma_x(t_1)\gamma_x(t_2)\right] \\ &\quad+ \mathbb{E}\left[\sum_{x,y\in\Phi_\mathrm{p}}^{\neq} \ell(\|x\|)\ell(\|y\|)\gamma_x(t_1)\gamma_y(t_2)\right], \end{aligned} \tag{21}$$

where in (a) terms with $x = y$ are separated from terms with $x \neq y$ and the expected value of fading $\mathbb{E}\big[h_x^2\big] = 1$ is substituted. The first of these expected values yields

$$\begin{aligned} \mathbb{E}\left[\sum_{x\in\Phi_\mathrm{p}} \ell^2(\|x\|)\gamma_x(t_1)\gamma_x(t_2)\right] &\overset{(a)}{=} \lambda_\mathrm{p} p_{12}\int_{\mathbb{R}^2}\ell^2(\|x\|)\,\mathrm{d}x \\ &= \lambda_\mathrm{p} p_{12}\,\frac{\alpha\pi}{\alpha-1}, \end{aligned} \tag{22}$$

where in (a) we apply Campbell's theorem. The second expectation of (21) gives

$$\begin{aligned} &\mathbb{E}\left[\sum_{x,y\in\Phi_\mathrm{p}}^{\neq} h_x^2\,\ell(\|x\|)h_y^2\,\ell(\|y\|)\gamma_x(t_1)\gamma_y(t_2)\right] \\ &\quad\overset{(a)}{=} \lambda_\mathrm{p}^2\int_{\mathbb{R}^2}\int_{\mathbb{R}^2}\ell(\|x\|)\,\ell(\|y\|)\,p_{1/2}(\|x-y\|)\,\mathrm{d}x\,\mathrm{d}y. \end{aligned} \tag{23}$$

In (a) we apply a basic property of the process, where $p_{1/2}(r)$ is the probability that two points at distance r are both retained each in an independent Matérn thinning, as derived in Lemma 4. Note that this expression is similar to (12) except that the second-order product density $\rho^{(2)}(2r)$ is substituted by $\lambda_\mathrm{p}^2\,p_{1/2}(2r)$. Applying similar steps as in the proof of Theorem 1 yields the result. □

Remarks.

- The covariance does not depend on fading as there is no m in the expression.

- Again, for $d \to 0$ the expression of $\mathrm{cov}[I_1, I_2]$ converges to the Poisson case: As mentioned in the remarks after Lemma 4, we have $p_{1/2}(r) \overset{r \geq 2d}{=} p_1^2$. Substituting this result into (23) leads to

$$\mathbb{E}\left[\sum_{x,y\in\Phi_\mathrm{p}}^{\neq} h_x^2\,\ell(\|x\|)h_y^2\,\ell(\|y\|)\gamma_x(t_1)\gamma_y(t_2)\right] = \left(\lambda\int_{\mathbb{R}^2}\ell(\|x\|)\,\mathrm{d}x\right)^2, \tag{24}$$

which is equal to $\mathbb{E}\,[I]^2$. Thus, we have

$$\mathrm{cov}[I_1, I_2] = \lambda_\mathrm{p} p_{12}\,\frac{\alpha\pi}{\alpha-1}. \tag{25}$$

4 Insights on Interference Correlation

So far we have derived expressions for the MPP and explained how these are generalizations of the PPP. Let us now plot and analyze the interference correlation of the Matérn network over certain parameters and compare these results to those of a Poisson network. For a fair comparison, the senders in the Poisson network are selected by an independent thinning of the PPP with probability p_1, leading to an intensity λ (which is equal to the density of senders in the Matérn network). This model resembles ALOHA as MAC protocol, where the sending probability is p_1. Both the CSMA and the ALOHA network model have the same expected value of interference $\mathbb{E}[I]$.[1]

If not stated otherwise, we use a path loss exponent $\alpha = 3$ and an intensity $\lambda_\mathrm{p} = 1$ for the PPP, hence having $0 \leq \lambda \leq 1$,

$$\rho\,[I_1, I_2] = \frac{\frac{\lambda(m+1)\,\alpha\pi}{m\,(\alpha-1)} + 8\pi\int_{\frac{d}{2}}^{\infty}\int_0^{\infty}\int_0^{2\pi}\frac{\ell(r(\cosh\mu+\cos\nu)\ell(r(\cosh\mu-\cos\nu)r^2(\cosh 2\mu-\cos 2\nu)}{2}\,\mathrm{d}\nu\,\mathrm{d}\mu\rho^{(2)}(2r)r\,\mathrm{d}r - \left(\frac{\lambda\alpha\pi}{\alpha-2}\right)^2}{\frac{\lambda_\mathrm{p}p_{12}\alpha\pi}{\alpha-1} + 8\pi\int_0^{\infty}\int_0^{\infty}\int_0^{2\pi}\frac{\ell(r(\cosh\mu+\cos\nu)\ell(r(\cosh\mu-\cos\nu)r^2(\cosh 2\mu-\cos 2\nu)}{2}\,\mathrm{d}\nu\,\mathrm{d}\mu p_{1/2}(2r)r\,\mathrm{d}r - \left(\frac{\lambda\alpha\pi}{\alpha-2}\right)^2}. \tag{26}$$

3.3 Correlation of Interference

The main result of this work is the calculation of the temporal correlation of interference. We show that there is a significant difference between PPPs and MPPs, and hence it is to be assumed that the correlation is also significantly different for ALOHA and carrier sensing MAC. This difference is important, as it can significantly impact the performance of retransmission protocols, diversity schemes, relaying, MIMO, and other techniques, unless they are considered in the particular design of these schemes [6], [7], [9], [20], [40].

Corollary 1 (Correlation of interference). *The temporal correlation of interference $\rho\,[I_1, I_2]$ at the origin o is given in (26).*

Proof. Pearson's correlation coefficient is defined as $\rho[I_1, I_2] = \frac{\mathrm{cov}[I_1,I_2]}{\sqrt{\mathrm{var}[I_1]\,\mathrm{var}[I_2]}}$. Hence, the result is obtained by dividing (20) by (11). □

Remarks.

- In the limit $d \to 0$ the temporal correlation of interference approaches the Poisson case with all potential senders transmitting:

$$\lim_{d\to 0}\rho\,[I_1, I_2] = \frac{m}{m+1}. \tag{27}$$

  In particular, for Rayleigh fading ($m = 1$) the correlation is $\lim_{d\to 0}\rho\,[I_1, I_2] \overset{m=1}{=} \frac{1}{2}$ and without fading we have $\lim_{m\to\infty}\lim_{d\to 0}\rho\,[I_1, I_2] = 1$.
- The temporal correlation of interference does not depend on the time period between I_i and I_j. In other words, for a given time instant t, the correlation $\rho[I_t, I_{t+i}]$ is the same for all $i \in \mathbb{Z}$. This result is relevant for retransmission protocols: If a transmission failed and has to be repeated, the sender can expect the same interference statistics independent of the time instant of the retransmission, i.e., a longer backoff does not increase the success probability in this model.

depending on the value of d. The default hard-core distance is $d = 1$.

All mathematical results have been crosschecked by simulations, showing a good match. Simulation results are only provided in Fig. 5, as showing further simulation results would not provide any additional information.

4.1 Impact of the Fraction of Sending Nodes

Fig. 2 shows the temporal correlation of interference for different fractions of nodes acting as interferers for both PPP and MPP. For the MPP, this correlation is calculated by numerical integration of the expression in Corollary 1 and is plotted over p_1 given in (2), varying the value of d. For the PPP, the scenario corresponds to Case (2,1,1) in the classification of [33]; the correlation is $\frac{qm}{m+1}$ with q being the fraction of active senders (see [8], [33]).

The most apparent observation is that PPP and MPP yield significantly different correlation curves. Hence, adopting a PPP to model a CSMA network may lead to the correct average interference but will incorrectly estimate the temporal dynamics in terms of correlation. Nevertheless, the curves of both models show the same trend: The correlations are strictly monotonically increasing with the fraction of senders and hit the same maximum value of $\frac{m}{m+1}$ for $\lambda \to \lambda_\mathrm{p}$, i.e., $p_1 \to 1$. In particular, the interference correlation of a PPP is neither an upper nor a lower bound for the one of an MPP. In general, it is higher for a small fraction of senders and lower for a high fraction. The crossing point heavily depends on the fading: weak fading (high m) shifts the crossing point toward small fractions of senders.

The implication of these properties on *practical networks with carrier sensing* are as follows: The correlation of interference might be very high over an unusually wide range of

1. Recall that, unlike for PPPs, conditioning on a point at the origin o does change the distribution of the rest of the process for MPPs, since there cannot be any point in its vicinity, i.e., $\mathcal{C}(o, d) \cap \Phi\backslash\{o\} = \emptyset$. In this work, we do not condition on having a point of the process being located at the origin o. This does not mean, however, that there is no receiver located at the origin (which anyway would not be part of the MPP that models the senders). It is just indicating, that this receiver has no sender assigned to it that is part of the MPP model.

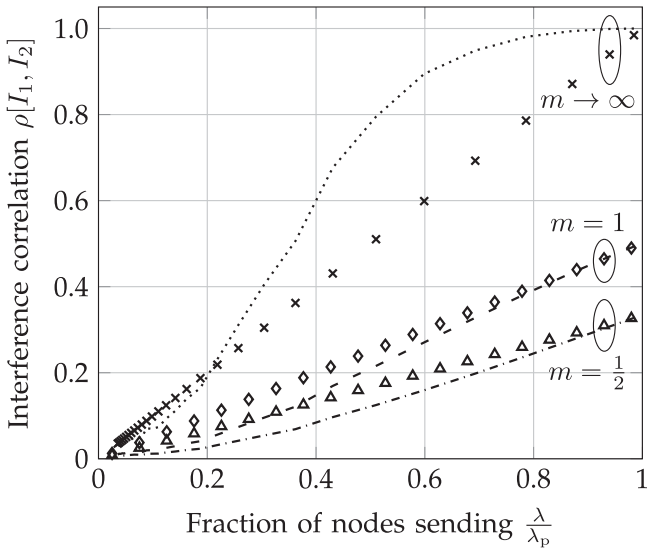

Fig. 2. Temporal correlation of interference over different sending probabilities. Lines indicate MPP and marks indicate PPP. Parameters are $\lambda_p = 1$ and $\alpha = 3$.

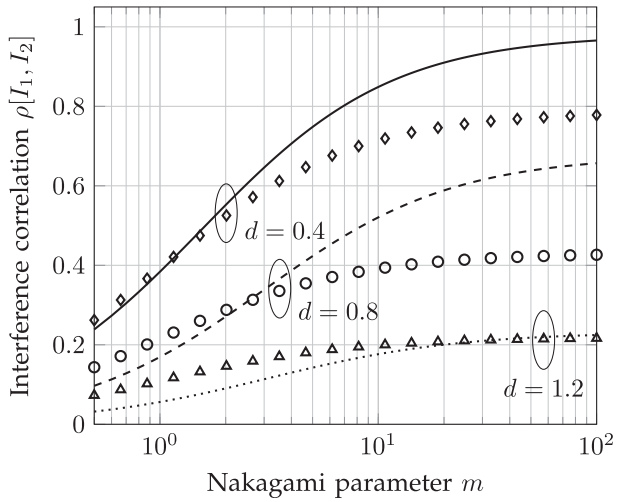

Fig. 3. Temporal correlation of interference over different fading strengths m. Lines indicate MPP and marks indicate PPP. Parameters are $\lambda_p = 1$ and $\alpha = 3$.

network parameters. For example, for high m, it is above 0.8 if on average more than half of the nodes send. Such high correlation is not predicted by the Poisson approximation of the network, for which the correlation is close to the sending probability (see [8], [33]). Hence, when limiting the analysis of a network with carrier sensing to the Poisson model, the resulting evaluation is incorrect, since high correlation can significantly impact the performance of retransmission diversity [6], cooperative relaying (see [6], [9], [20]), and methods to predict interference [41]. The design of the network has to be adjusted accordingly based on the knowledge of interference correlation.

4.2 Impact of the Channel

Fig. 3 shows how the interference correlation depends on the severeness of fading represented by m. It is well known for PPPs that the correlation of interference decreases with increasing fading (decreasing m). The reason is that severe fading leads to a high variance of interference but does not change the covariance. We observe the same qualitative behavior for MPPs. All curves flatten out for increasing m, and in case of no fading ($m \to \infty$), the correlation converges to a value that depends on λ and d, which is plotted in Fig. 2 (dotted curve). The value of m determines as to which of the two models shows a higher correlation. Interference correlation is not automatically higher for Matérn networks compared to Poisson networks. Instead, whether it is higher or lower can only be determined by knowing or estimating the harshness of fading. The highest gaps between Matérn and Poisson networks occur for weak or no fading (high m). In this case, carrier sensing typically shows higher correlation than ALOHA, whereas the opposite is the case for weak fading.

Considering *practical networks with carrier sensing*, our results imply that the fading statistics of the channel have to be considered for designing protocols. Even if a channel estimation in conjunction with methods that compensate fading is applied, this does not reduce the impact of fading on interference correlation. In other terms, even tough the effect of fading on the reception power can be compensated, its effect on correlation remains. Depending on the time scale of interference, this result has different implications for the network: In case of slowly changing interference, retransmissions might have to be delayed or diversity schemes might have to be designed differently, or otherwise their effectivity is decreased (see [6], [7], [20]).

Fig. 4 shows that the interference correlation in the MPP depends on the path loss exponent α, while it is independent of α for PPPs. This dependence is, however, very small: For low α (close to 2), the correlation is slightly smaller than for higher values. For values $\alpha \geq 3$, there is almost no change in correlation when further increasing α.

4.3 Impact of the Sensing Range

Fig. 5 shows that the interference correlation decreases with increasing hard-core distance d and eventually vanishes for $d \to \infty$. The reason for this behavior is that d determines the number of senders. A higher d models a more sensitive sensing, which implies fewer simultaneously sending nodes that are further apart. If a higher fraction of nodes send, naturally the temporal correlation is higher, and vice versa. This is already known for PPPs with a linear relation between fraction of senders and correlation [8]. For MPPs, we have the same qualitative behavior but with a non-linear relation between fraction of senders and correlation.

Overall, we conclude that sensing sensitivity determines the interference correlation: If the sensing is very sensitive, few nodes are sending, thus the correlation is small. If the sensing is nonsensitive, correlation increases up to the point without sensing, which eventually yields slotted ALOHA. In mathematical terms, this is modeled by $d \to 0$ leading to a PPP.

For *practical networks with carrier sensing* these results imply the following: On the one hand, if the sensing is more sensitive, i.e., it reacts already to slight increases in interference, both the expected interference power and interference correlation are lower. On the other hand, also the spatial reuse is reduced as fewer transmissions can take place simultaneously with the higher hard-core distance d. Hence, the question arises on the optimal value for

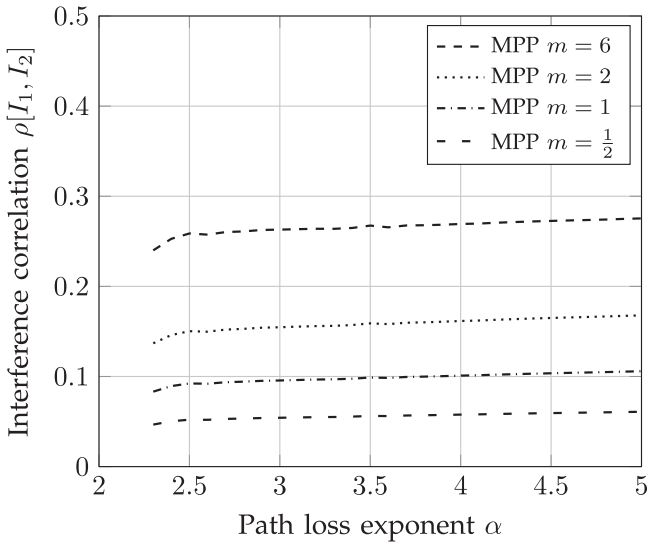

Fig. 4. Temporal correlation of interference over different path loss exponents α. Parameters are $\lambda_p = 1$ and $d = 1$. Numerical integrations are unstable for $\alpha < 2.3$.

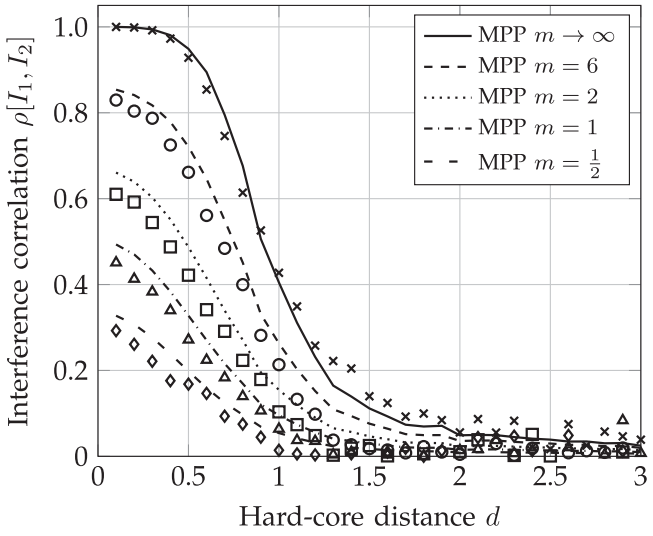

Fig. 5. Temporal correlation of interference over different hard-core distances d. Parameters are $\lambda_p = 1$ and $\alpha = 3$. Lines indicate analytic results and marks indicate simulations. The glitches in the curves (e.g., close to $d = 2$) are due to instabilities in numerical integrations.

d to maximize the overall network throughput. This question cannot be addressed with the tools at hand as it would require an analysis of outage, which is outside the scope of this work.

4.4 Impact of the Node Intensity

Fig. 6 plots the interference correlation of a Matérn network over the intensity λ_p of the PPP from which the MPP is derived from. It shows a strong decrease of correlation for increasing λ_p. This is in contrast to Poisson networks, where the intensity has no impact on interference correlation. The main reason for this dependency in MPPs is that d does not scale with λ_p. Hence, for a higher density, a smaller fraction of nodes is allowed to send, since they are on average closer packed, which reduces the retainment probability p_1. Indeed, from (2), we can conclude that p_1 monotonically decreases with increasing λ_p.

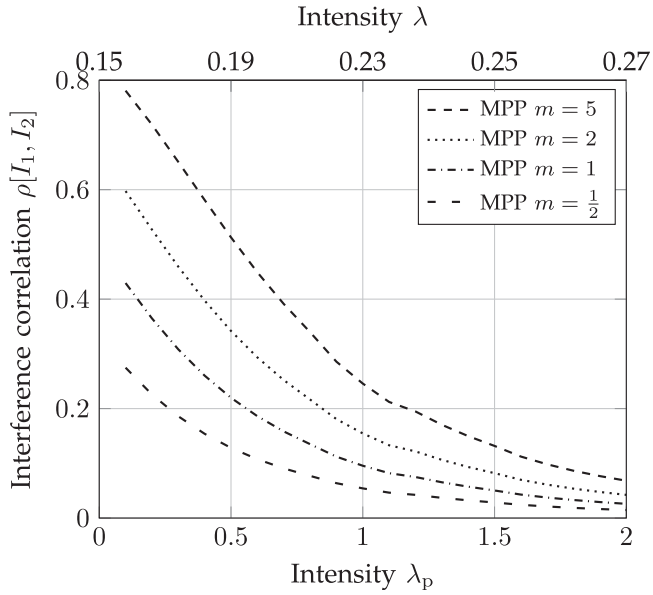

Fig. 6. Temporal correlation of interference over different intensities λ_p of the PPP to which Matérn thinning is applied. Parameters are $d = 1$ and $\alpha = 3$. The upper axis label shows the intensity λ of the MPP. It increases with λ_p and is upper bounded by $\frac{1}{d^2\pi}$.

This result has the following implications on *practical networks with carrier sensing*: For a dense network with high λ_p, only a small fraction of nodes can transmit simultaneously due to the carrier sensing mechanism—most nodes are in backoff. In contrast, for a sparse network with small λ_p a high fraction of nodes is transmitting simultaneously. For well-chosen system parameters, the expected interference is similar over this range of λ_p implying that the number of sending nodes per unit area is not affected under appropriate parameters. In combination, these results imply that the correlation of interference in sparse networks is higher than in dense networks even though the outage probability can be similar due to proper medium access control. In turn, it is to be expected that the performance of techniques such as cooperative relaying highly depends on the density of the network; related results for Poisson networks confirm this conjecture [20], whereas a detailed analysis on this topic for Matérn networks is left to future work.

5 Conclusions

This article contributes to interference calculus in wireless networks with emphasis on the dynamics of interference in Matérn networks with Nakagami fading. We derived and analyzed previously unknown expressions for the variance and covariance of interference power and calculated the correlation coefficient.

We proved that the interference dynamics is significantly different in networks with carrier sensing than in networks without sensing. An important difference is that the interference correlation in Matérn networks depends on the intensity of the underlying point process, which is irrelevant in Poisson networks. The path loss exponent has almost no influence on interference correlation in both types of networks. These results demonstrate the limits of the commonly used Poisson network model. At the same time, our results highlight the potential of the Matérn point process as a viable model for

networks with carrier sensing: it approximates important aspects of CSMA networks while remaining tractable to a certain extend.

The knowledge on interference dynamics has value in the design of real networks. For example, interference correlation can significantly influence the gains of diversity and can be a building block in the design of interference prediction techniques.

APPENDIX A
PROOFS OF LEMMAS

Proof of Lemma 2. Let $m_{x,1}$ and $m_{x,2}$ with $0 \leq m_{x,1}, m_{x,2} \leq 1$ denote the marks of $x \in \Phi_\mathrm{p}$ in the first and the second thinning, respectively. We consider the point process $\Phi_{t^2} = \{y \in \Phi_\mathrm{p} \,|\, m_{y,1} < m_{x,1} \vee m_{y,2} < m_{x,2}\}$ of all points having a mark being smaller than $m_{x,1}$ in the first or smaller than $m_{x,2}$ in the second thinning. The probability that an arbitrary point is in this set is $m_{x,1} + m_{x,2} - m_{x,1}m_{x,2}$ by the inclusion-exclusion principle. Hence, the point process Φ_{t^2} has the intensity $(m_{x,1} + m_{x,2} - m_{x,1}m_{x,2})\,\lambda$. The probability that no point of Φ_{t^2} is located in $b(x,d)$ is then given by the void probability of the process Φ_{t^2}, i.e., by $\exp\big(-(m_{x,1} + m_{x,2} - m_{x,1}m_{x,2})\lambda\, d^2\pi\big)$. Therefore, the probability that x is retained twice is

$$p_{12} = \int_0^1 \int_0^1 e^{-(m_{x,1}+m_{x,2}-m_{x,1}m_{x,2})\,\lambda d^2\pi} \mathrm{d}m_{x,1}\,\mathrm{d}m_{x,2}. \tag{28}$$

Solving these integrals yields the result. □

Proof of Lemma 3. Similar derivations as the following can be found in [39]. We present a version of the proof that aligns to our notation. Let us consider two points $x, y \in \Phi_\mathrm{p}$ at distance $\|x-y\| = r > 0$. If $r \leq d$, it is impossible that both points are retained due to the definition of a hard-core point process. Hence, let $r > d$ in the following. Recall that whether x and y are retained depends on the marks of the points in $\mathcal{C}(x,d)$ and $\mathcal{C}(y,d)$, respectively. If $r < 2d$, these circles overlap and we subdivide them into three areas: $A_c := \mathcal{C}(x,d) \cap \mathcal{C}(y,d)$ is the common area, $A_x := \mathcal{C}(x,d) \backslash \mathcal{C}(y,d)$ and $A_y := \mathcal{C}(y,d) \backslash \mathcal{C}(x,d)$ are the non-common areas. The sizes of these areas are [1]

$$|A_c| = \gamma_d(r) \overset{r \leq 2d}{=} 2d^2 \arccos\Big(\frac{r}{2d}\Big) - \frac{r}{2}\sqrt{4d^2 - r^2} \tag{29}$$

$$|A_x| = |A_y| = d^2\pi - \gamma_d(r). \tag{30}$$

For $r \geq 2d$ the common area vanishes giving $|A_c| = 0$. The area covered by at least one of the circles is

$$|A_x \cup A_y| = \Gamma_d(r) = 2d^2\pi - \gamma_d(r). \tag{31}$$

Let m_x and m_y denote the marks of x and y, respectively. To retain both x and y, the following three conditions have to hold: First, A_x must not contain any point from $z \in \Phi_\mathrm{p}$ with $m_z < m_x$. For given m_x, the probability for it is $\exp(-m_x\,\lambda_\mathrm{p}\,|A_x|)$, similarly to the proofs of Lemmas 1 and 2. Second, A_y must not contain any $z \in \Phi_\mathrm{p}$ with $m_z < m_y$, which happens with probability $\exp(-m_y\,\lambda_\mathrm{p}\,|A_y|)$. Third, the common area A_c must not contain any $z \in \Phi_\mathrm{p}$ with $m_z < \max(m_x, m_y)$, which has the probability $\exp(-\max(m_x, m_y)\,\lambda_\mathrm{p}\,|A_c|)$. Overall, the probability that both x and y are retained is

$$\begin{aligned} p_{1/1}(r) = \int_0^1 \int_0^1 \exp\big(&-(m_x + m_y)\,\lambda_\mathrm{p}\,|A_x| \\ &- \max(m_x, m_y)\,\lambda_\mathrm{p}\,|A_c|\big)\,\mathrm{d}m_x\,\mathrm{d}m_y. \end{aligned} \tag{32}$$

Solving these integrals yields the result. □

Proof of Lemma 4. Let us consider two points $x, y \in \Phi_\mathrm{p}$ at distance $\|x-y\| = r > 0$. We define the areas A_c, A_x, and A_y as given in (29) and (30) of the proof of Lemma 3.

Let us assume $r > d$. For given m_x and m_y, there should be no point $z \in \Phi_\mathrm{p}$ with $m_z < m_x$ in the area A_x at the first thinning and no point $z \in \Phi_\mathrm{p}$ with $m_z < m_y$ in A_y at the second thinning. The probability for these events is given by

$$\exp\Big(-(m_x + m_y)\,\lambda_\mathrm{p}\,\big(d^2\pi - \gamma_d(r)\big)\Big). \tag{33}$$

The probability that there is no point $z \in \Phi_\mathrm{p}$ in A_c with $m_z < m_x$ at the first or $m_z < m_y$ at the second thinning is

$$\exp\big(-(m_x + m_y - m_x m_y)\,\lambda_\mathrm{p}\,\gamma_d(r)\big), \tag{34}$$

similar to the proof of Lemma 2. Integrating over the product of these two expressions yields

$$\begin{aligned} p_{1/2}(r) \overset{r \geq d}{=} \int_0^1 \int_0^1 \exp\Big(&-(m_x + m_y)\,\lambda_\mathrm{p}\,\big(d^2\pi - \gamma_d(r)\big) \\ &- (m_x + m_y - m_x m_y)\,\lambda_\mathrm{p}\,\gamma_d(r)\Big)\,\mathrm{d}m_x\,\mathrm{d}m_y. \end{aligned} \tag{35}$$

Next, we assume that $r < d$. In this case, the derivation of $p_{1/2}(r)$ is similar to the previous case, except $x \in A_c$ in the first thinning and $y \in A_c$ in the second one. Hence, x has to have a higher mark than y in the first thinning, and y a higher mark than x in the second thinning. These two events have the probabilities $(1 - m_x)$ and $(1 - m_y)$ respectively, leading to

$$\begin{aligned} p_{1/2}(r) \overset{r \leq d}{=} \int_0^1 \int_0^1 \exp\Big(&-(m_x + m_y)\,\lambda_\mathrm{p}\,\big(d^2\pi - \gamma_d(r)\big) \\ &- (m_x + m_y - m_x m_y)\,\lambda_\mathrm{p}\,\gamma_d(r)\Big) \\ &(1 - m_x)(1 - m_y)\,\mathrm{d}m_x\,\mathrm{d}m_y. \end{aligned} \tag{36}$$

Solving the integrals in (35) and (36) yields the result. □

Proof of Lemma 5. The derivation of the expected interference is similar to its version for PPPs [8], [33]. All nodes in the set $\Phi \subseteq \Phi_\mathrm{p}$ are considered to be interferers. Hence, the expected value of interference is calculated by applying Campbell's theorem yielding

$$\begin{aligned} \mathbb{E}[I] &= \mathbb{E}\left[\sum_{x \in \Phi_\mathrm{p}} h_x^2\,\ell(\|x\|)\gamma_x(t)\right] \\ &= \lambda_\mathrm{p} \int_{\mathbb{R}^2} \ell(\|x\|)\,\mathbb{E}\big[h_x^2\big]\,\mathbb{E}[\gamma_x(t)]\,\mathrm{d}x \\ &= \lambda_\mathrm{p} p_1\,\frac{\alpha\pi}{\alpha - 2}. \end{aligned} \tag{37}$$

The expected value of the indicator function $\gamma_x(t)$ does neither depend on x nor on t. This is because we do not consider any nodes to be placed at certain locations (e.g., the origin), which implies that we do not adopt the Palm distribution of the MPP. Substituting (3) into this expression gives the result. □

ACKNOWLEDGMENTS

This work has been supported by the Austrian Science Fund (FWF) under grant P24480-N15 (Dynamics of Interference in Wireless Networks), and by the K-project DeSSnet (Dependable, secure and time-aware sensor networks), which is funded within the context of COMET–Competence Centers for Excellent Technologies by the Austrian Ministry for Transport, Innovation and Technology (BMVIT), the Federal Ministry for Digital and Economic Affairs (BMDW), and the federal states of Styria and Carinthia; the COMET program is conducted by the Austrian Research Promotion Agency (FFG).

REFERENCES

[1] D. Stoyan, W. S. Kendall, and J. Mecke, *Stochastic Geometry and Its Applications*. Hoboken, NJ, USA: Wiley, 1995.
[2] M. Haenggi, J. G. Andrews, F. Baccelli, O. Dousse, and M. Franceschetti, "Stochastic geometry and random graphs for the analysis and design of wireless networks," *IEEE J. Sel. Areas Commun.*, vol. 27, no. 7, pp. 1029–1046, Sep. 2009.
[3] F. Baccelli and B. Błaszczyszyn, "Stochastic Geometry and Wireless Networks, Volume II: Applications," *Foundations and Trends in Networking*, vol. 4, no. 1–2, pp. 1–312.
[4] M. Haenggi, *Stochastic Geometry for Wireless Networks*. Cambridge, U.K.: Cambridge Univ. Press, 2013.
[5] U. Schilcher, S. Toumpis, M. Haenggi, A. Crismani, G. Brandner, and C. Bettstetter, "Interference functionals in Poisson networks," *IEEE Trans. Inf. Theory*, vol. 62, no. 1, pp. 370–383, Jan. 2016.
[6] M. Haenggi and R. Smarandache, "Diversity polynomials for the analysis of temporal correlations in wireless networks," *IEEE Trans. Wireless Commun.*, vol. 12, no. 11, pp. 5940–5951, Nov. 2013.
[7] U. Schilcher, S. Toumpis, A. Crismani, G. Brandner, and C. Bettstetter, "How does interference dynamics influence packet delivery in cooperative relaying?" in *Proc. ACM/IEEE Int. Conf. Model. Anal. Simul. Wireless Mobile Syst.*, Nov. 2013, pp. 347–354.
[8] R. Ganti and M. Haenggi, "Spatial and temporal correlation of the interference in ALOHA ad hoc networks," *IEEE Commun. Lett.*, vol. 13, no. 9, pp. 631–633, Sep. 2009.
[9] R. Tanbourgi, H. S. Dhillon, J. G. Andrews, and F. K. Jondral, "Effect of spatial interference correlation on the performance of maximum ratio combining," *IEEE Trans. Wireless Commun.*, vol. 13, no. 6, pp. 3307–3316, Jun. 2014.
[10] *IEEE Standard for Information Technology: Telecommunications and Information Exchange between Systems Local and Metropolitan Area Networks: Specific Requirements - Part II: Wireless LAN Medium Access Control (MAC) and Physical Layer (PHY) Specifications*, IEEE Std 802.11–2016, Dec. 2016.
[11] B. Kaufman, J. Lilleberg, and B. Aazhang, "Spectrum sharing scheme between cellular users and ad-hoc device-to-device users," *IEEE Trans. Wireless Commun.*, vol. 12, no. 3, pp. 1038–1049, Mar. 2013.
[12] Q. Ye, M. Al-Shalash, C. Caramanis, and J. G. Andrews, "Resource optimization in device-to-device cellular systems using time-frequency hopping," *IEEE Trans. Wireless Commun.*, vol. 13, no. 10, pp. 5467–5480, Oct. 2014.
[13] H. ElSawy, E. Hossain, and M.-S. Alouini, "Analytical modeling of mode selection and power control for underlay D2D communication in cellular networks," *IEEE Trans. Commun.*, vol. 62, no. 11, pp. 4147–4161, Nov. 2014.
[14] X. Lin, J. G. Andrews, and A. Ghosh, "Spectrum sharing for device-to-device communication in cellular networks," *IEEE Trans. Wireless Commun.*, vol. 13, no. 12, pp. 6727–6740, Dec. 2014.
[15] J. F. Schmidt, M. K. Atiq, U. Schilcher, and C. Bettstetter, "Underlay device-to-device communications in LTE-A: Uplink or downlink?" in *Proc. IEEE Int. Symp. Personal Indoor Mobile Radio Commun.*, 2015, pp. 1692–1696.
[16] H. Q. Nguyen, F. Baccelli, and D. Kofman, "A stochastic geometry analysis of dense IEEE 802.11 networks," in *Proc. IEEE Int. Conf. Comput. Commun.*, May 2007, pp. 1199–1207.
[17] B. Matérn, *Spatial Variation*. Berlin, Germany: Springer Lecture Notes in Statistics, 1986.
[18] M. Haenggi, "Mean interference in hard-core wireless networks," *IEEE Commun. Lett.*, vol. 15, no. 8, pp. 792–794, Aug. 2011.
[19] F. Tobagi and L. Kleinrock, "Packet switching in radio channels: Part II - The hidden terminal problem in carrier sense multiple-access and the busy-tone solution," *IEEE Trans. Commun.*, vol. TC-23, no. 12, pp. 1417–1433, Dec. 1975.
[20] A. Crismani, S. Toumpis, U. Schilcher, G. Brandner, and C. Bettstetter, "Cooperative relaying under spatially and temporally correlated interference," *IEEE Trans. Veh. Technol.*, vol. 64, no. 10, pp. 4655–4669, Oct. 2015.
[21] "Feasibility study on licensed-assisted access to unlicensed spectrum," *3GPP TR 36.889 v13.0.0*, Malmö, Sweden, 2015.
[22] H. J. Kwon, J. Jeon, A. Bhorkar, Q. Ye, H. Harada, Y. Jiang, L. Liu, S. Nagata, B. L. Ng, T. Novlan, J. Oh, and W. Yi, "Licensed-assisted access to unlicensed spectrum in LTE release 13," *IEEE Commun. Mag.*, vol. 55, no. 2, pp. 201–207, Feb. 2017.
[23] A. Mukherjee, J. F. Cheng, S. Falahati, H. Koorapaty, D. H. Kang, R. Karaki, L. Falconetti, and D. Larsson, "Licensed-assisted access LTE: Coexistence with IEEE 802.11 and the evolution toward 5G," *IEEE Commun. Mag.*, vol. 54, no. 6, pp. 50–57, Jun. 2016.
[24] B. Cho, K. Koufos, and R. Jantti, "Bounding the mean interference in Matérn type II hard-core wireless networks," *IEEE Commun. Lett.*, vol. 2, no. 5, pp. 563–566, Oct. 2013.
[25] R. K. Ganti, J. G. Andrews, and M. Haenggi, "High-SIR transmission capacity of wireless networks with general fading and node distribution," *IEEE Trans. Inf. Theory*, vol. 57, no. 5, pp. 3100–3116, May 2011.
[26] G. Alfano, M. Garetto, and E. Leonardi, "New insights into the stochastic geometry analysis of dense CSMA networks," in *Proc. IEEE Conf. Comput. Commun.*, Apr. 2011, pp. 2642–2650.
[27] J. G. Andrews, T. Bai, M. N. Kulkarni, A. Alkhateeb, A. K. Gupta, and R. W. Heath, "Modeling and analyzing millimeter wave cellular systems," *IEEE Trans. Commun.*, vol. 65, no. 1, pp. 403–430, Jan. 2017.
[28] N. Deng, W. Zhou, and M. Haenggi, "The Ginibre point process as a model for wireless networks with repulsion," *IEEE Trans. Wireless Commun.*, vol. 14, no. 1, pp. 107–121, Jan. 2015.
[29] D. B. Taylor, H. S. Dhillon, T. D. Novlan, and J. G. Andrews, "Pairwise interaction processes for modeling cellular network topology," in *Proc. IEEE Global Commun. Conf.*, Dec. 2012, pp. 4524–4529.
[30] G. L. Torrisi and E. Leonardi, "Large deviations of the interference in the Ginibre network model," *Stoch. Syst.*, vol. 4, pp. 173–205, 2014.
[31] F. Lagum, S. S. Szyszkowicz, and H. Yanikomeroglu, "Quantifying the regularity of perturbed triangular lattices using CoV-based metrics for modeling the locations of base stations in HetNets," in *Proc. IEEE Veh. Technol. Conf.*, Sep. 2016, pp. 1–5.
[32] A. Busson and G. Chelius, "Point processes for interference modeling in CSMA/CA ad-hoc networks," in *Proc. ACM Symp. Perform. Eval. Wireless Ad Hoc Sensor Ubiquitous Netw.*, Oct. 2009, pp. 33–40.
[33] U. Schilcher, C. Bettstetter, and G. Brandner, "Temporal correlation of interference in wireless networks with Rayleigh block fading," *IEEE Trans. Mobile Comput.*, vol. 11, no. 12, pp. 2109–2120, Dec. 2012.
[34] S. Krishnan and H. S. Dhillon, "Spatio-temporal interference correlation and joint coverage in cellular networks," *IEEE Trans. Wireless Commun.*, vol. 16, no. 9, pp. 5659–5672, Sep. 2017.
[35] M. Haenggi, "The meta distribution of the SIR in Poisson bipolar and cellular networks," *IEEE Trans. Wireless Commun.*, vol. 15, no. 4, pp. 2577–2589, Apr. 2016.
[36] F. Baccelli, B. Blaszczyszyn, and P. Muhlethaler, "An ALOHA protocol for multihop mobile wireless networks," *IEEE Trans. Inf. Theory*, vol. 52, no. 2, pp. 421–436, Feb. 2006.
[37] M. Nakagami, "The m-distribution — A general formula of intensity distribution of rapid fading," in *Proc. Statistical Methods Radio Wave Propagation*, Jun. 1958, pp. 3–36.
[38] M. Shafi, A. F. Molisch, P. J. Smith, T. Haustein, P. Zhu, P. D. Silva, F. Tufvesson, A. Benjebbour, and G. Wunder, "5G: A tutorial overview of standards, trials, challenges, deployment, and practice," *IEEE J. Sel. Areas Commun.*, vol. 35, no. 6, pp. 1201–1221, Jun. 2017.

[39] D. Stoyan and H. Stoyan, "On one of Matérn's hard-core point process models," *Math. Nachr.*, vol. 122, no. 1, pp. 205–214, 1985.
[40] A. Crismani, U. Schilcher, S. Toumpis, G. Brandner, and C. Bettstetter, "Packet travel times in wireless relay chains under spatially and temporally dependent interference," in *Proc. IEEE Int. Conf. Commun.*, Jun. 2014, pp. 2002–2008.
[41] M. K. Atiq, U. Schilcher, J. F. Schmidt, and C. Bettstetter, "Semi-blind interference prediction in wireless networks," in *Proc. ACM/IEEE Int. Symp. Model. Anal. Simul. Wirel. Netw.*, Nov. 2017, pp. 19–23.

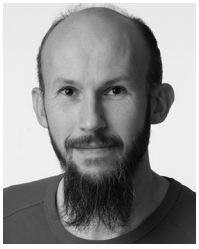

Udo Schilcher received the two Dipl-Ing degrees with distinction in applied computing and mathematics from the University of Klagenfurt, 2005 and 2006, respectively. From 2005 to 2017, he was a research staff member with the Institute of Networked and Embedded Systems, University of Klagenfurt. His doctoral thesis on inhomogeneous node distributions and interference correlation in wireless networks and has been awarded with a Dr. techn. degree with distinction in 2011. After his graduation, from 2011 he held senior positions with the Institute of Networked and Embedded Systems, University of Klagenfurt, and at Lakeside Labs GmbH. His main interests are interference dynamics and spatial node distributions in wireless networks, and stochastic geometry. He received a best paper award from the IEEE Vehicular Technology Society.

Jorge F. Schmidt received the BSc and DSc degrees in electrical engineering from the Universidad Nacional del Sur, Bahía Blanca, Argentina, in 2005 and 2011, respectively. From 2012 to 2014, he was a postdoctoral fellow in the Signal Processing and Communications Laboratory, University of Vigo, Spain. In 2014, he joined the Institute of Networked and Embedded Systems group, University of Klagenfurt, Austria. Since 2016, he has also been a senior researcher at Lakeside Labs GmbH, Austria. His main research interests lie in the area of statistical signal processing and interference modeling and management for wireless communications systems. He received a best paper award from the ACM SIGSIM.

Christian Bettstetter (S'98-M'04-SM'09) received the Dipl-Ing degree in 1998 and the Dr-Ing degree (summa cum laude), in 2004, both in electrical and information engineering from Technische Universität München (TUM), Munich, Germany. He was a research and teaching staff member with the Institute of Communication Networks, TUM, until 2003. From 2003 to 2005, he was a senior researcher with DOCOMO Euro-Labs. He has been a professor with the University of Klagenfurt, Austria, since 2005, and founding director of the Institute of Networked and Embedded Systems since 2007. He is also the founding scientific director of Lakeside Labs, a research company on self-organizing networked systems. He is a senior member of the IEEE.